Progress In Electromagnetics Research B, Vol. 1, 95–113, 2008

SMALL SIZE KA-BAND DISTRIBUTED MEMS PHASE SHIFTERS USING INDUCTORS

S. Afrang and B. Y. Majlis

Institute of Microengineering and Nanoelectronics (IMEN)
University Kebangsaan Malaysia
43600 Bangi, Selangor, Malaysia

Abstract—MEMS phase shifter has been developed using inductors. The design consists of a CPW line capacitively and inductively loaded by the periodic set of inductors and electrostatic force actuated MEMS switches as capacitors. By applying a single bias voltage on the line, the characteristic impedance can be changed, which in turn changes the phase velocity of the line and creates a true time delay phase shift. The governing equations for the impedance and loss are derived. The ABCD matrix is defined for a unit cell and multi-cell DMTL phase shifter to extract scattering parameters equations. The MEMS switch is actuated by a 39 voltage waveform using a high resistance bias line. Estimated spring constant and switching time is 22 N/m and 3 μs, respectively. The structure is designed for Ka-band frequency range. The acceptable frequency range for the design containing 21 cells is between 26 GHz and 27 GHz and optimum condition occurs at 26.3 GHz. For the whole structure and optimum condition the un actuated position results in a return loss -16 dB and insertion loss of -1.65 dB. The actuated position results in a return loss -12.5 dB and insertion loss of -1.6 dB. The phase shift for the whole structure is 190 degree. The optimum condition can be easily changed by modifying the design parameters. The spacing in the proposed structures is $S = 250\,\mu$m. The structure is also low loss. The length and the loss per bit with the phase shift of 270° are decreased by 37.5 percent and 21 percent respectively.

1. INTRODUCTION

Electronic phase shifters demonstrated high insertion loss [1, 2]. But, Analog phase shifters using coplanar waveguide (CPW) lines with distributed microelectromechanical system (MEMS) bridges

demonstrated broad-band characteristics with low loss [3]. However, since there was a limit on the control range of the bridge height before the bridge snaps, the analog phase shifter showed relatively small phase shift. This problem was solved by operating the MEMS bridges in the digital mode [4–11], where two distinct capacitance states (ON and OFF) were defined with a high ratio. Digital phase shifters with this approach allow large phase shift and low sensitivity to electrical noise. In the published CPW digital phase shifters [4, 5], a small metal-insulator-metal (MIM) capacitor or metal-air-metal (MAM) [10, 11] in series with the MEMS bridge capacitor was used to reduce the total shunt capacitance seen by the line, resulting in an acceptable return loss for both switching states over a wide band.

This work presents a new concept of distributed MEMS true time delay phase shifters using both inductors and capacitors. As it is known, the inductor changes the phase of a signal same as the capacitor. In our distributed MEMS transmission line (DMTL) design, MEMS switches and inductors are used to change loading capacitance and inductance on a high-impedance t-line such that the return loss is within an acceptable range for the two phase states (with the MEMS switches in the up- and down-state positions). Traditionally, commercially available phase shifters are based on ferrite materials, p-i-n diodes or FET switches but they consume power more than MEMS based phase shifters. There is a drawback using MEMS phase shifters. MEMS based phase shifters have large size. It is essential that the area of a RF MEMS phase shifter be reduced. The advantages of decreased area are much higher part count per wafer, easier hermetic packaging and much lower coast. The goal of the design in this paper is to decrease the size of the structure by maintaining the maximum amount of phase shift with the minimum amount of insertion loss and with a low return loss per unit cell.

2. MODELING AND DESIGN EQUATIONS

Coplanar wave-guide (CPW) transmission line has been used for the design. Figure 1 shows a unit cell MEMS phase shifter on a glass substrate.

There are two MEMS bridges, two capacitors and one inductor in the structure. One of the bridges is in the shunt configuration and connects the inductor to the AC capacitor. Another bridge is inline and defined in the CPW center conductor. The inductor consists of two segments: The main segment is placed in the gap, inside the ground plane, while the shunt MEMS bridge makes other segment of the inductor. One end of the inductor is connected to the RF connector

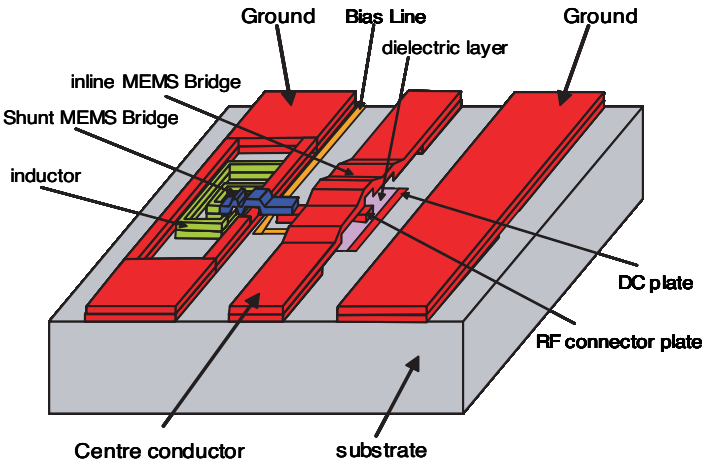

Figure 1. The schematic of proposed DMTL phase shifter (unit cell).

plate and another end is grounded. There are two capacitors under the inline MEMS bridge. The plate under the dielectric layer together with the inline MEMS bridge makes DC capacitor. The DC voltage is applied to this capacitor using a single high-resistance bias line. Another capacitor is AC capacitor. The plate on the dielectric layer (RF connector plate) together with the inline MEMS bridge makes AC capacitor in the up state (un-actuated) position. The AC capacitor only exists in the up-state position.

Figure 2 shows the equivalent circuit of the proposed structure in the up state position. In this circuit, the distributed parameters for the impedance of transmission line have been used where L_t, C_t and R_t are per unit length inductance, capacitance and resistance of the transmission line respectively, and "s" is the periodic separation. R_I, L_I and C_I are the series resistance, inductance and the capacitance of the coil respectively. The AC capacitance of inline MEMS bridge is

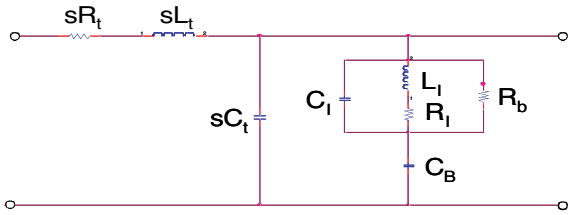

Figure 2. The equivalent circuit in the up state position.

shown by C_B. The bias line resistance R_b is in parallel with inductor.

When the voltage is applied to the inline MEMS bridge, the bridge moves down and makes required contact with the RF connector plate. Therefore, the ungrounded end of the inductor is connected to the center conductor. In this condition, the inductor is connected in parallel to the center conductor. Figure 3 shows the equivalent circuit of the structure in the down state (actuated) position.

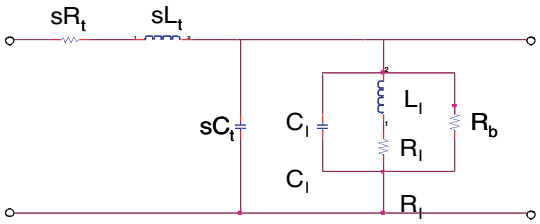

Figure 3. The equivalent circuit in the down state position.

Figure 4 shows the distributed circuit model for the phase shifter. It consists of a unit cell which is cascaded multiple times in a t line circuit. Each unit cell is capable of certain amount of phase shift and by adding more cells the total phase shift increases by a factor of the number of cells.

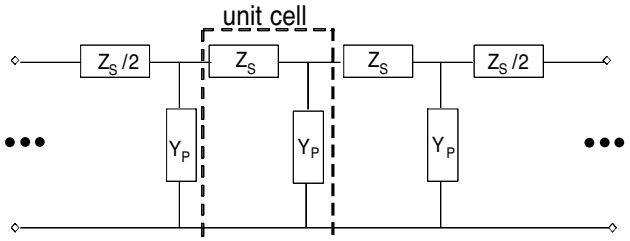

Figure 4. The general model for a distributed transmission line.

Considering Figure 4, the characteristic impedance for a distributed line is given by [12],

$$Z_o = \sqrt{\frac{Z_s}{Y_p}}\sqrt{1 + \frac{Z_s Y_p}{4}} \tag{1}$$

By assuming $R_t = 0$ and using general model for the proposed structure

in the up state position the loaded t-line impedance is given by:

$$Z_u = \sqrt{\frac{-\omega \cdot sL_t R_q \cdot C_U + jsL_t\left(1-\omega^2 \cdot L_I \cdot C_U\right)}{-\omega(sC_tR_qC_u + C_IC_BR_q) + j[sC_t(1-\omega^2L_IC_U) + C_B(1-\omega^2C_IL_I)]}} \sqrt{1+\frac{-\omega^2 sL_t[sC_t(1-\omega^2L_IC_U)+C_B(1-\omega^2C_IL_I)+j\omega R_q(sC_tC_U+C_BC_I)]}{4\left(1-\omega^2 \cdot L_I \cdot C_U + j\omega R_q \cdot C_U\right)}} \tag{2}$$

Where,

$$R_q = R_I + (\omega L_I)^2/R_b \tag{3}$$

and,

$$C_U = C_I + C_B \tag{4}$$

As equation (2) shows, there are two resonance frequencies in the up state position and are given by:

$$f_{r1(up)} = \frac{1}{2\pi\sqrt{L_I \cdot C_U}} \tag{5}$$

$$f_{r2(up)} = \frac{1}{2\pi\sqrt{L_I \cdot C_I}} \tag{6}$$

Using general model for the proposed structure and by considering Figure 3 the loaded t-line impedance in the down state position is given by:

$$Z_d = \sqrt{\frac{-\omega^2 L_I \cdot sL_t + j\omega R_q \cdot sL_t}{1-\omega^2 L_I \cdot C_d + j\omega R_q \cdot C_d}} \times \sqrt{1+\frac{-\omega^2 \cdot sL_t \cdot R_q \cdot C_d + j\omega \cdot sL_t(1-\omega^2 \cdot L_I C_d)}{4(R_q + j\omega L_I)}} \tag{7}$$

where

$$C_d = sC_t + C_I \tag{8}$$

As equation (7) shows, there is one resonance frequencies in the down state position and is given by:

$$f_{r(down)} = \frac{1}{2\pi\sqrt{L_I C_d}} \tag{9}$$

As it is known, in the capacitive type MEMS phase shifters, the impedance value is fixed below the Bragg frequency, while from equations (2) and (7) it can be seen that the characteristic impedance in the proposed structure changes with frequency.

The per unit length inductance and capacitance of a transmission line are determined to be [13],

$$L_t = \frac{\sqrt{\varepsilon_{r,eff}} \cdot Z_o}{c} \tag{10}$$

$$C_t = \frac{\sqrt{\varepsilon_{r,eff}}}{Z_o \cdot c} \tag{11}$$

Where, $\varepsilon_{r,eff}$ is the effective dielectric constant of the unloaded line and $c/\sqrt{\varepsilon_{r,eff}}$ is the guided velocity of the high-impedance CPW line without any loading.

The pull down voltage and the switching time are found to be [13],

$$V_p \cong \sqrt{\frac{8kg_0^3}{27\varepsilon A}}. \tag{12}$$

$$t = 3.67\frac{V_p}{V_s\omega_0}, \tag{13}$$

Where, k, and ω_0 are the spring constant and resonance frequency of the MEMS bridge, respectively. V_s, g_0 and A, are the applied voltage, gap distance and the area between the DC plate and MEMS bridge, respectively.

For a beam over a CPW line with the center conductor a third of the length of the beam, the spring constant is given by [13],

$$K = \frac{32Ewt^3}{l^3}\left(\frac{27}{49}\right) + \frac{8\sigma(1-v)wt}{l}\left(\frac{3}{5}\right) \tag{14}$$

Where $E, w, l, t, v,$ and σ are Young's modulus, width, length, thickness, Poisson's ratio and biaxial residual stress of the MEMS bridge respectively.

The resonance frequency for the fixed-fixed beam bridge is given by [14],

$$\omega^2 = \frac{\int_0^l EI\left[\frac{d^2y(x)}{dx^2}\right]^2 dx}{\int_0^l \rho A[y(x)]^2 dx} \tag{15}$$

Where, ρ and A are the density and cross sectional area of the bridge and I and $y(x)$ are second moment of area of the cross-section and

the deflection at any distance x along the length of the bridge and are given by,

$$I = \frac{wt^3}{12} \tag{16}$$

$$y(x) = \frac{Fx^2}{48EI}(4x - 3l) \tag{17}$$

3. DERIVATION OF SCATTERING PARAMETERS AND LOSS COMPONENTS

The distributed line phase shifter can be conveniently analyzed using the $ABCD$ matrices. To derive S_{11} in terms of $ABCD$-parameters, the equivalent circuit in Figure 5 has been used. In this circuit, Z_{O2} is a matched transmission line. Z_{O1} is the characteristic impedance of the lossy transmission line. The length of the lossy transmission line determines the periodic separation. The structure is placed over this line. The term $(G_L + jB_L)$ is the shunt load.

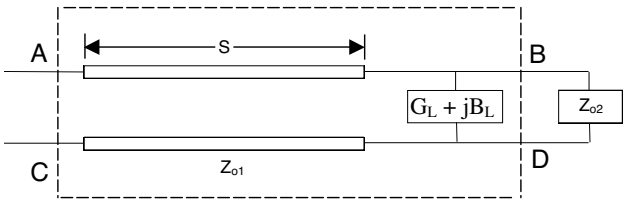

Figure 5. Circuit for derivation of S_{11}.

S_{11} in terms of $ABCD$-parameters of the structure and matched transmission line Z_{O2} is as following [15]:

$$S_{11} = \frac{A + B \cdot Y_{O2} - C \cdot Z_{O2} - D}{A + B \cdot Y_{O2} + C \cdot Z_{O2} + D} \tag{18}$$

The $ABCD$ matrix of the lossy transmission line is given by:

$$\begin{bmatrix} A & B \\ C & D \end{bmatrix} = \begin{bmatrix} \cosh(\gamma \cdot s) & Z_{O1} \cdot \sin(\gamma \cdot s) \\ Y_{O1} \cdot \sinh(\gamma \cdot s) & \cosh(\gamma \cdot s) \end{bmatrix} \tag{19}$$

$$\gamma = \alpha + j\beta \tag{20}$$

Where, γ, α and β are the complex propagation constant, attenuation and the phase constant of the transmission line respectively.

The $ABCD$ matrix of the shunt load is given by:

$$\begin{bmatrix} A & B \\ C & D \end{bmatrix} = \begin{bmatrix} 1 & 0 \\ G_L + jB_L & 1 \end{bmatrix} \tag{21}$$

By considering the serial combination of inductor and ac capacitance of MEMS bridge, G_L and B_L for the structure in the up state position is given by:

$$G_{L(up)} = \frac{-\omega^2 C_B C_I R_I [1-\omega^2 L(C_B+C_I)] + \omega^2 C_B R_I (C_I+C_B)(1-\omega^2 L C_I)}{[1-\omega^2 L(C_B+C_I)]^2 + \omega^2 R_I^2 (C_I+C_B)^2} \tag{22}$$

$$B_{L(up)} = \frac{\omega C_B (1-\omega^2 L C_I)(1-\omega^2 L(C_B+C_I) + \omega^3 C_B C_I R_I^2 (C_I+C_B)}{[1-\omega^2 L(C_B+C_I)]^2 + \omega^2 R_I^2 (C_I+C_B)^2} \tag{23}$$

For the design in the down state position the shunt load consists of only inductor. Therefore, G_L and B_L for the structure in the actuated position are as following:

$$G_{L(down} = \frac{R_I}{R_I^2 + \omega^2 L_I^2} \tag{24}$$

$$B_{L(down} = \frac{\omega R_I^2 C_I - \omega L_I (1-\omega^2 L_I C_I)}{R_I^2 + \omega^2 L_I^2} \tag{25}$$

The overall $ABCD$ matrix of the structure is obtained as:

$$\begin{bmatrix} A & B \\ C & D \end{bmatrix} = \begin{bmatrix} \cosh(\gamma \cdot s) & Z_{O1} \cdot \sinh(\gamma \cdot s) \\ Y_{O1} \cdot \sinh(\gamma \cdot s) & \cosh(\gamma \cdot s) \end{bmatrix} \cdot \begin{bmatrix} 1 & 0 \\ G_L + jB_L & 1 \end{bmatrix} \tag{26}$$

To derive S_{21} in terms of $ABCD$-parameters, the equivalent circuit in Figure 6 has been used. The source impedance Z_{O2} must be included in the calculation to separate incident and reflected waves. S_{21} in terms of $ABCD$-parameters is as following:

$$S_{21} = \frac{2}{A + B \cdot Y_{O2} + C \cdot Z_{O2} + D} \tag{27}$$

The $ABCD$ matrix of the structure has not been changed and is obtained from equation (26). There are two contributors to the

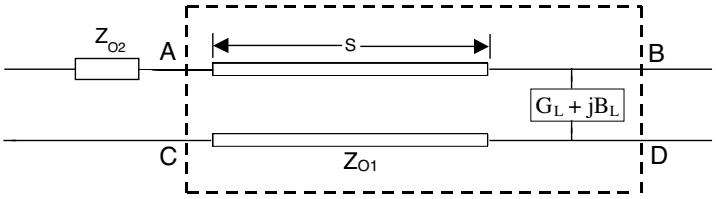

Figure 6. Circuit for derivation of S_{21}.

insertion loss of the structure. They consist of conductor loss and Q loss in the shunt loading inductor. The inductor Q loss is the combined loss of inductor resistor and bias line resistor. The bias lines have a significant effect on the overall insertion loss performance of the phase shifter because they decrease the effective Q of the structure.

The lossy static inductor is modeled as, R_S, in series with L_I (or a resistance R_P, in parallel with L_I). The inductor Q can be written as:

$$Q = \frac{\omega \cdot L_I}{R_S} = \frac{R_P}{\omega \cdot L_I} \tag{28}$$

(28) where,

$$R_S = \frac{(\omega \cdot L_I)^2}{R_P} \tag{29}$$

Bias line resistance is in parallel with inductor. Therefore, considering the equation (29) the total resistance in the shunt section is equal to the series resistance, R_I, due to the Q of the inductor, plus equivalent series bias line resistance,

$$R_q = R_I + (\omega L_I)^2 / R_b \tag{30}$$

There are two methods to calculate the loss of the structure. One method is to extract the loss from S-parameters. The S_{21} does not necessarily indicate power loss in the unit cell, but can simply be due to the reflected power from the structure. The loss of the structure is better derived from the S-parameters as:

$$\text{Loss} = 10 \log |S_{21}|^2 - 10 \log(1 - |S_{11}|^2) \quad \text{dB} \tag{31}$$

In another method consider a transmission line which is represented by a series inductance and resistance per unit length, L_t and R_t, and by a shunt capacitance and admittance per unit length, C_t and G_t, respectively, the attenuation constant α is given by [16]

$$\alpha = \frac{R_t}{2Z} + \frac{G_t Z}{2} \quad \frac{Np}{unilength} \tag{32}$$

In a planar transmission line such as CPW, R_t represents the transmission line conductor loss, and G_t represents the dielectric loss. The corresponding t-line loss α for the proposed structure is:

$$\alpha \cong 8.686 \left(\frac{R_t}{2Z_o} + \frac{G_L \cdot Z_o}{2} \right) \quad \text{dB/section} \tag{33}$$

where, G_L represents the shunt loaded loss in the up or down state position and Z_o is the system impedance. The structure is

placed within this system [15]. Most TEM transmission line systems have 50-ohm characteristic impedance so that when the characteristic impedance is not specified, 50 ohm is assumed. The transmission-line loss equation related to physical parameters of the unloaded CPW line is found from a conformal mapping technique, and is given by Hoffmann [17]

$$\alpha_c = F_f \frac{8.686 R_s \sqrt{\varepsilon_{r,eff}}}{4\eta S K(k) K(k')(1-k^2)} \times \left[\frac{2S}{W}\left(\pi + \ln\left[\frac{4\pi W(1-k)}{t(1+k)}\right]\right) + 2\left(\pi + \ln\left[\frac{4\pi S(1-k)}{t(1+k)}\right]\right)\right] \text{ dB/m} \tag{34}$$

where F_f is a fudge factor ($F_f = 1.47$ for 30 GHz) since equation (34) follows the correct trend for loss vs. impedance. It should be noted that this equation significantly underestimates the measured loss of the CPW line on Pyrex. The resistive per unit length is given by [18]:

$$R = \frac{\rho}{\delta \cdot W} \tag{35}$$

Where, ρ (Ω-m) is the metal resistivity, w is the width of the line, and δ is the skin depth given by:

$$\delta = \sqrt{\frac{\rho}{\pi \cdot \mu \cdot f}} \tag{36}$$

Where, μ is the permeability of free space. In practice, the resistivity of plated materials are around 1.3–1.5 times higher than bulk values presented by equation (35). For evaporated materials the resistivity is about 2 time, more than bulk values.

4. KA-BAND DMTL PHASE SHIFTER DESIGN

Figure 7 shows the magnitude of the characteristic impedances for a unit cell in the up and down state position using equations (2) and (7). From Figure 7, it is seen that in the up state position and as a result of RLC series configuration around $f_{r1(up)}$, the structure behaves as a capacitor in the frequencies lower than $f_{r1(up)}$. Therefore, for the frequencies lower than $f_{r1(up)}$ increases the electrical length of the transmission line. It can also be seen that parallel RLC model in the down state position shortens the electrical length of the transmission line. Thus, switching from a pair of capacitance in the up state position to inductive elements in the down state position effectively increases the electrical length, thereby causing a differential phase shift.

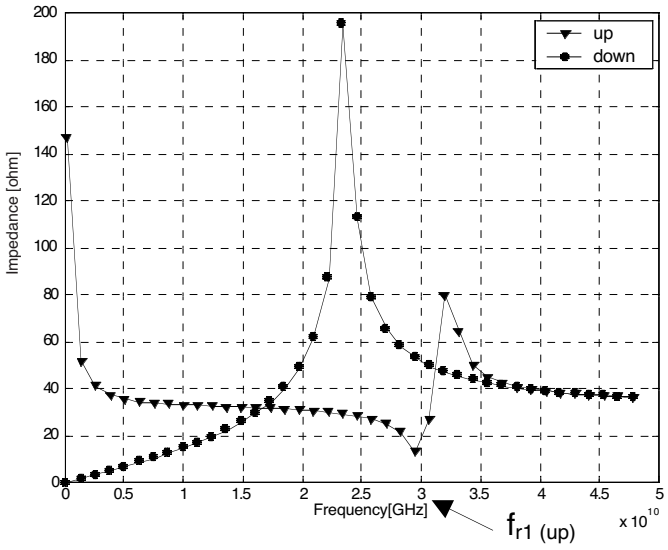

Figure 7. Characteristic impedance diagrams in the up and down state position.

The first step in the design is to determine the impedance of the transmission line before it is loaded. In the capacitor type MEMS phase shifters the varactor can only serve to lower the impedance in both up and down state position. Therefore the impedance of the transmission line must be greater than the highest load impedance. In the proposed structure the bridge capacitor in series with the inductor after loading decrease the impedance of the transmission line in the up state position. Whereas in the down state positions the inductor in parallel with the transmission line capacitor increase the impedance of the transmission line around the resonance frequency. Therefore, the impedance of the transmission line must be between the loaded impedances. On the other hand to achieve acceptable return loss, the loaded impedances in the up and down state position should be close to the system impedance.

The next step is to determine the inductor parameters. Consider for example the inductance of the inductor is $L_P = 1\,\text{nH}$. Considering two segments of the inductor and using the greenhouse formulas [19], the case of the $1\frac{1}{4}$ turn planar rectangular coil is achieved. The track width and external diameter of the coil is $30\,\mu\text{m}$ and $200\,\mu\text{m}$ respectively. This planar coil together with the shunt MEMS bridge with the length of $440\,\mu\text{m}$, make the total added inductor in the structure. The low frequency value of planar inductors is

generally obtained using the greenhouse formulas. However, these formulas provide only approximate values. In general, L_I and R_I are fitted using low frequency simulations, while C_I is fitted around the resonance frequency of the planar inductor. R_I can also be calculated using equation (35). These calculations and simulations result in an inductance 0.95 nH, $C_I = 16$ fF and $R_I = 2\,\Omega$ around Ka-band frequencies.

For the design, $f_{r1(up)}$ is a critical point and determine the frequency band. The sign of the phase changes from negative in the frequencies lower than $f_{r1(up)}$ to positive for the frequencies higher than $f_{r1(up)}$. The desired area are the frequencies lower than $f_{r1(up)}$. Therefore, if we consider K_a-band design, we can select for example 30 GHz for $f_{r1(up)}$ Now, by considering the equations (4), (5), the capacitance of the inline MEMS bridge capacitor is 14 fF.

From equations (8) and (9) it can be seen that the transmission line parameters and spacing affect the resonant frequency and as a result change the impedance of the structure in the down state position much more than up state position. As mentioned the desired area are the frequencies lower than $f_{r1(up)}$. Therefore, to have the desired impedance, the resonance frequency in the down state position should be sufficiently less than $f_{r1(up)}$. In the optimum condition $Z_o = 40\,\Omega(G/W/G = 15/150/15\,\mu$m, $\varepsilon_{r,eff} = 2.36)$ and $S = 250\,\mu$m suit to achieve desired loaded impedances. The silicon-chrome (Si/Cr, 90/10) is used as a high resistive material. Cell to cell resistance is 50 KΩ. Effectively, the shunt load "see" two of these resistances in parallel because there are two bias lines attached to each cell.

5. UNIT CELL SIMULATION AND CALCULATION

The unit cell of the proposed K_a-band MEMS phase shifter is simulated and calculated using EM3D and MATLAB softwares respectively. The coplanar waveguide line with the dimensions of $G/W/G = 15/150/15\,\mu$m and the gold with the resistivity of $\rho = 2.35\,n\Omega$-m for the line is used. The substrate is a 400 μm thick glass with the dielectric permittivity of $\varepsilon_{r,eff} = 2.36$. The inductor calculation and simulation results in an inductance of $L_I = 0.95$ nH, a resistivity $R_I = 2\,\Omega$ and the capacitance of $C_I = 16$ fF. The inline bridge capacitance is $C_B = 14$ fF. The mechanical and geometrical parameters of the structure are listed in Table 1.

Figure 8 shows simulation and calculation results of the return loss (S_{11}) in the up and down state position. From these diagrams, it can be seen that there is a maximum return loss in the up state position. Maximum return loss is a result of minimum impedance at

Table 1. Materials and geometrical parameters (Sizes are in micrometers).

Parameter	Value
Young modulus, E_{AL} (GPa)	68.85
Poisson's ratio, v_{AL}	0.36
Density (g/cm^3)	2.7
Permittivity of air (F/m)	$8.85 \cdot 10^{-12}$
Length of the beam	200
Width of the beam	150
Initial gap	2.2
Thickness of the beam	1
Thickness of the dielectric layer	0.3

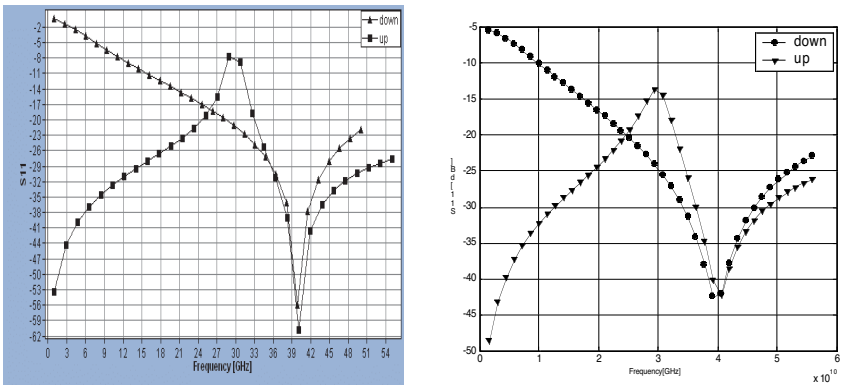

(a) (b)

Figure 8. Simulation and calculation results of the return loss (S_{11}) in the up and down state position. (a) Simulation diagrams. (b) Calculation diagrams.

the first resonance frequency (30 GHz) in the up state position.

Figure 9 shows simulation and calculation results of the insertion loss (S_{21}) in the up and down state position. These diagrams show high insertion loss as a result of low impedance characteristic for the frequencies lower than $f_{r(down)}$ in the down state position. These diagrams also show maximum insertion loss as a result of minimum impedance at the first resonance frequency in the up state position.

Figure 10 shows simulation and calculation results of the phase

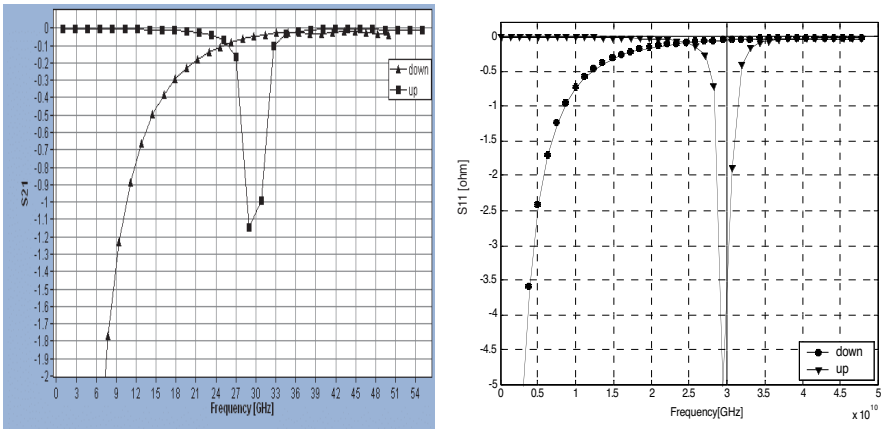

(a) (b)

Figure 9. Simulation results of the insertion loss (S_{11}) in the up and down state position. (a) Simulation diagrams. (b) Calculation diagrams.

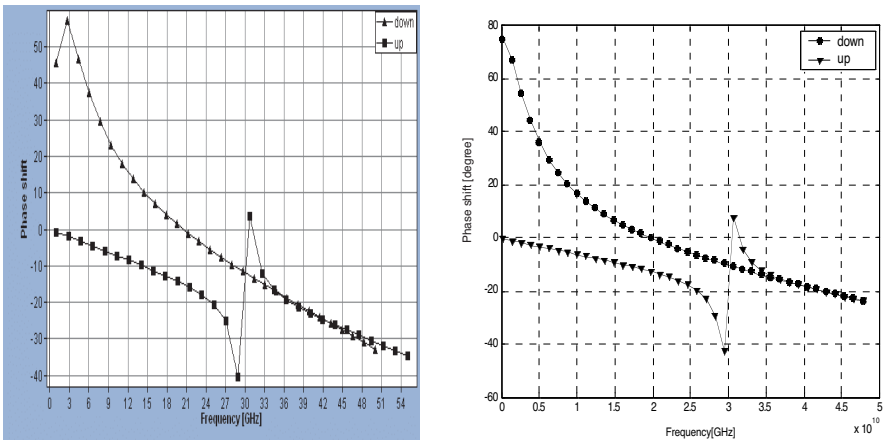

(a) (b)

Figure 10. Simulation and calculation results of the phase angle in the up and down state position. (a) Simulation diagrams. (b) Calculation diagrams.

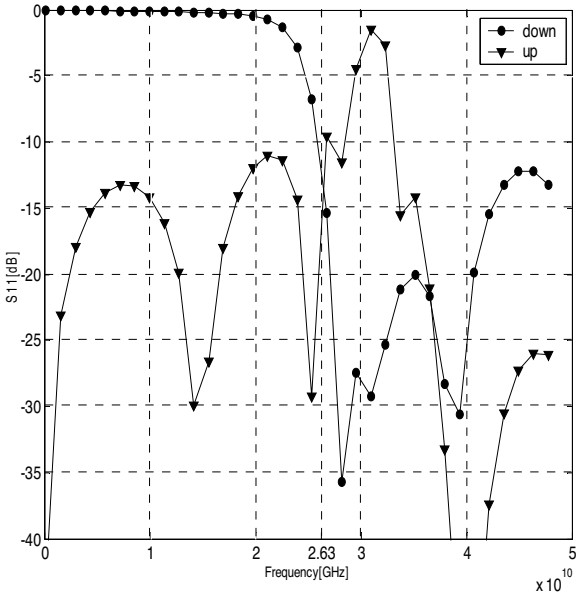

Figure 11. Return loss (S_{11}) diagrams of 21 cascaded cells in the up and down state position (calculated using MATLAB).

difference between up and down state position. It is seen, that $f_{r1(up)}$ is a critical point and the sign of the phase changes from negative in the frequencies lower than $f_{r1(up)}$ to positive for the frequencies higher than $f_{r1(up)}$.

Mechanical behavior of the structure is simulated using intellisuite software. Simulation results show the actuation voltage of 39 volt. Considering the equation (12) the calculation results in a actuation 28 volt. This equation is based on parallel plates. MEMS bridge is one of the plates. When the actuation voltage is applied, the bridge bends. Beam bending causes unequally electrostatic force that is not considered in the equation.

6. MULTI-CELL DESIGN CONSIDERATIONS

The $ABCD$ matrix is defined so that pairs can be cascaded by simple multiplication and equations. For multi-cell structure shown in Figure 4, each cell is represented by an $ABCD$ matrix and the cells are combined using $ABCD$ matrices. The cells are cascaded by multiplication working from right to left. At the end of the calculation, the entire circuit is represented by one $ABCD$ matrix, which can

be converted to measurable S-parameters using equations (18) and (27). For the proposed K_a-band MEMS phase shifter, one bit MEMS phase shifter containing 21 cascaded cells is calculated using MATLAB software. The calculated S-parameters and phase diagrams in the up and down state positions are shown in Figures 11, 12 and 13. From these figures it can be seen that the acceptable frequency range for the design is between 26 GHz and 27 GHz. and the optimum point for S_{11}, S_{21} and phase shift is around 26.3 GHz. The return loss between 26 GHz and 27 GHz is better than -10 dB. Considering the desired frequency and equations (32) and (34), the transmission line resistance is $R_t = 340\,\Omega/\mathrm{m}$. Finally, the loss can be calculated using equation (33).

Table 2. Calculation and simulation results of the unit cell at 26.3 GHz.

	S_{11}	S_{21}	S_{11}	S_{21}	Phase shift	spacing	Bias line loss	Bias line loss	R_t plus R_l loss	R_t Plus R_l loss	V_s	switching time
	dB	dB	dB	dB	degree	μm	dB	dB	dB	dB	v	μs
	up	up	down	down			up	down	up	down		
Proposed structure (simulation)	-17	-0.13	-18	-0.08	15.5	250	-	-	0.074	0.014	39 (σ=0)	3
Proposed structure (calculation)	-17	-0.17	-20	-0.07	14	250	0.035	0.01	0.076	0.016	28 (σ=0)	2.3

Table 3. Calculation results of 21 cells with the phase shift of 270° at 26.3 GHz.

	S_{11}(up)	S_{21}(up)	S_{11}(down)	S_{21}(down)	Phase shift	Length
	dB	dB	dB	dB	Degree	mm
Proposed structure (calculation)	-16	-1.65	-12.5	-1.6	265	5.25
Capacitive type[8]	-	-	-11.5	-2.1	270	8.4

Table 2 shows calculation and simulation results of the unit cell at 26.3 GHz. This table also compares obtained results with the unit cell of capacitive type.

Table 3 compares one bit results of the proposed structure with the capacitive type. As it is seen, to achieve 270° phase shift, the length per bit and the loss of the proposed structure are decreased by 37.5 percent and 21 percent respectively.

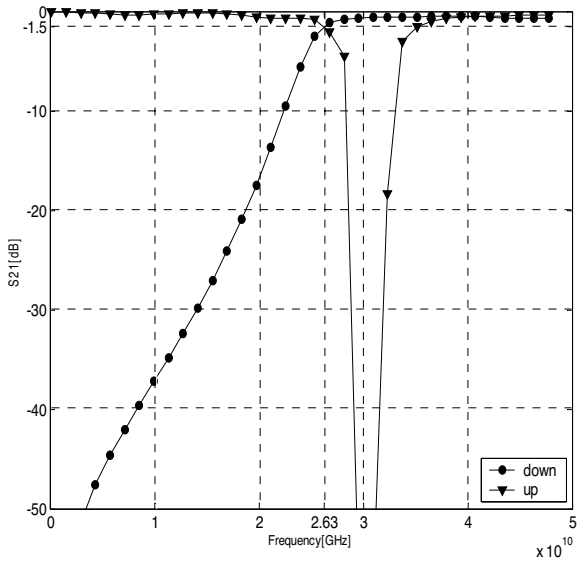

Figure 12. Insertion loss (S_{21}) diagrams of 21 cascaded cells in the up and down state position (calculated using MATLAB).

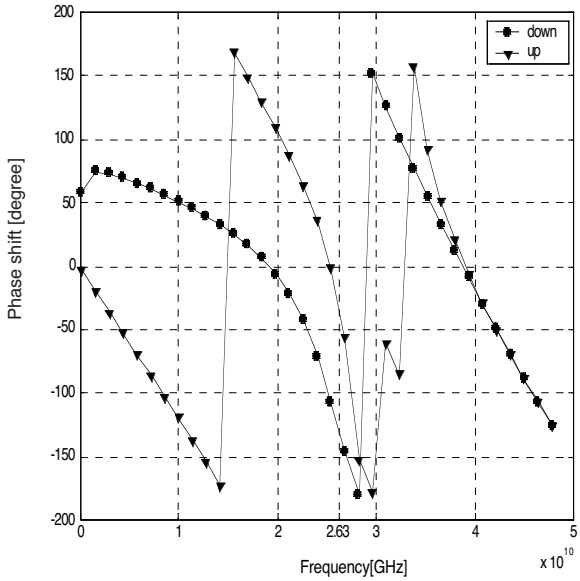

Figure 13. Phase diagrams of 21 cascaded cells in the up and down state position (calculated using MATLAB).

7. CONCLUSION

This paper presented small size and low loss K_a-band distributed MEMS phase shifter. The concept of MEMS phase shifter using inductor was introduced and governing equations on impedance, loss and scattering parameters were derived. For a multi-cell containing 21 cells at 26.3 GHz, the Un-actuated calculation resulted in a reflection coefficient -16 dB, and an insertion loss of -1.65 dB. The actuated calculation resulted in a reflection coefficient -12.5 dB, and an insertion loss of -1.6 dB. The phase shift for the whole structure was 265 degree. The spacing in the proposed structures was $S = 250\times10^{-6}$. The length and the loss per bit with the phase shift of 265° were decreased by 37.5 percent and 21 percent respectively.

ACKNOWLEDGMENT

This work has been supported by the Malaysian Ministry of Science, Technology and innovation under the project title "MEMS devices and sensing microstructures 03-02-02-0015-SR0003/07-01".

REFERENCES

1. Wang, Z., B. Yan, R. M. Xu, and Y. Guo, "Design of a Ku band six bit phase shifter using periodically loaded-line and switched-line with loaded-line," *Progress In Electromagnetics Research*, PIER 76, 369–379, 2007.
2. Akdagli, A., K. Guney, and B. Babayigit, "Clonal selection algorithm for design of reconfigurable antenna array with discrete phase shifters," *Journal of Electromagnetic Waves and Applications*, Vol. 21, No. 2, 215–227, 2007.
3. Barker, N. S. and G. M. Rebeiz, "Distributed MEMS true-time delay phase shifters and wide-band switches," *IEEE Trans. Microwave Theory and Tech.*, Vol. 46, No. 1, 1881–1890, 1998.
4. Borgioli, A., Y. Liu, A. S. Nagra, and R. A. York, "Low-loss distributed MEMS phase shifter," *IEEE Microwave Guided Wave Lett.*, Vol. 10, 7–9, 2000.
5. Hayden, J. S. and G. M. Rebeiz, "2-bit MEMS distributed X-band phase shifters," *IEEE Microwave Guided Wave Lett.*, Vol. 10, 540–542, 2000.
6. Liu, Y., A. Borgioli, A. S. Nagra, and R. A. York, "K-band 3-bit low-loss distributed MEMS phase shifter," *IEEE Microwave Guided Wave Lett.*, Vol. 10, 415–417, 2000.

7. Hayden, J. S., A. Makczewski, J. Kleber, C. L. Goldsmith, and G. M. Rebeiz, "2 and 4-bit DC-18 GHz microstrip MEMS distributed phase shifters," *IEEE MTT-S Int. Microwave Symp. Dig.*, 219–222, May 2001.
8. Pillans, B., S. Eshelman, A. Malczewski, J. Ehmke, and C. L. Goldsmith, "Ka-band RF MEMS phase shifters," *IEEE Microwave Guided Wave Lett.*, Vol. 9, 520–522, 1999.
9. Kim, M., J. B. Hacker, R. E. Mihailovich, and J. F. DeNatale, "A DC-to-40 GHz four-bit RF MEMS true-time delay network," *IEEE Microwave Wireless Comp. Lett.*, Vol. 11, 56–58, 2001.
10. Hayden, J. S. and G. M. Rebeiz, "Very low-loss distributed X-band and Ka-band MEMS phase shifters using metal-air-metal capacitors," *IEEE Trans. on Microwave Theory and Tech.*, Vol. 51, No. 1, 309–314, 2003.
11. Hung, J.-J., L. Dussopt, and G. M. Rebeiz, "Distributed 2- and 3-bit W-band MEMS phase shifters on glass substrates," *IEEE Trans. on Microwave Theory and Tech.*, Vol. 52, No. 2, 600–606, 2004.
12. Hayden, J. S., "High-performance digital X-band and Ka-band distributed MEMS phase shifters," Ph.D. thesis, University of Michigan, Ann Arbor, 2002.
13. Barker, N. S., "Distributed MEMS transmission lines," Ph.D. thesis, University of Michigan, Ann Arbor, 1999.
14. Rao, S. S., *Mechanical Vibrations*, Addison-Wesley Publishing Company, 1995.
15. Wolff, E. A., *Microwave Engineering and Systems Applications*, John Wiley & Sons Publication, 1988.
16. Pozar, D. M., *Microwave Engineering*, Addison-Wesley Publishing Company, Reading, MA, 1990.
17. Hoffmann, R. K., *Handbook of Microwave Integrated Circuits*, Artech House, Norwood, MA, 1987.
18. Rebeiz, G. M., *RF MEMS Theory Design and Technology*, John Wiley & Sons Publication, 2003.
19. Greenhouse, H. M., "Design of planar rectangular microelectronic inductors," *IEEE Transaction on Parts Hybrids and Packaging*, Vol. PHP-10, No. 2, 101–109, 1974.